

Durham Research Online

Deposited in DRO:

22 February 2019

Version of attached file:

Published Version

Peer-review status of attached file:

Peer-reviewed

Citation for published item:

Chala, Mikael and Ramos, Maria and Spannowsky, Michael (2019) 'Gravitational wave and collider probes of a triplet Higgs sector with a low cutoff.', *European physical journal C.*, 79 (2). p. 156.

Further information on publisher's website:

<https://doi.org/10.1140/epjc/s10052-019-6655-1>

Publisher's copyright statement:

This article is distributed under the terms of the Creative Commons Attribution 4.0 International License (<http://creativecommons.org/licenses/by/4.0/>), which permits unrestricted use, distribution, and reproduction in any medium, provided you give appropriate credit to the original author(s) and the source, provide a link to the Creative Commons license, and indicate if changes were made. Funded by SCOAP3.

Additional information:

Use policy

The full-text may be used and/or reproduced, and given to third parties in any format or medium, without prior permission or charge, for personal research or study, educational, or not-for-profit purposes provided that:

- a full bibliographic reference is made to the original source
- a [link](#) is made to the metadata record in DRO
- the full-text is not changed in any way

The full-text must not be sold in any format or medium without the formal permission of the copyright holders.

Please consult the [full DRO policy](#) for further details.



Gravitational wave and collider probes of a triplet Higgs sector with a low cutoff

Mikael Chala¹, Maria Ramos^{2,a} , Michael Spannowsky¹

¹ Institute of Particle Physics Phenomenology, Physics Department, Durham University, Durham DH1 3LE, UK

² Laboratório de Instrumentação e Física Experimental de Partículas, Departamento de Física da Universidade do Minho, Campus de Gualtar, 4710-057 Braga, Portugal

Received: 13 December 2018 / Accepted: 4 February 2019
 © The Author(s) 2019

Abstract We study the scalar triplet extension of the standard model with a low cutoff, preventing large corrections to the quadratic masses that would otherwise worsen the hierarchy problem. We explore the reach of LISA to test the parameter space region of the scalar potential (not yet excluded by Higgs to diphoton measurements) in which the electroweak phase transition is strongly first-order and produces sizeable gravitational waves. We also demonstrate that the collider phenomenology of the model is drastically different from its renormalizable counterpart. We study the reach of the LHC in ongoing searches and project bounds for the HL-LHC. Likewise, we develop a dedicated analysis to test the key but still unexplored signature of pair-production of charged scalars decaying to third-generation quarks: $pp \rightarrow t\bar{b}(\bar{t}b), b\bar{b}$. These results apply straightforwardly to other extensions of the Higgs sector such as the 2HDM/MSSM.

Contents

| | |
|------------------------------------|-------|
| 1 Introduction | |
| 2 Model | |
| 3 The electroweak phase transition | |
| 4 Collider signatures | |
| 5 LHC sensitivity | |
| 6 Conclusions | |
| Appendix A: Loop functions | |
| References | |

^a e-mail: mariaramos@lip.pt

1 Introduction

Hyperchargeless triplet scalars Φ arise in a variety of models of new physics. They include

- (i) theories of grand unification (GUT), where scalar multiplets, often transforming in the adjoint representation of the GUT group, break spontaneously the GUT symmetry. A simple example is the **24** in $SU(5)$, which decomposes as $(1, 1)_0 + (1, \mathbf{3})_0 + \dots$ under the Standard Model (SM) gauge group $SU(3)_c \times SU(2)_L \times U(1)_Y$, therefore delivering a scalar triplet. Likewise, the **45** representation of $SO(10)$ contains the **24** of $SU(5)$ and therefore a SM triplet as well.
- (ii) Supersymmetric (SUSY) models. As a matter of fact, the triplet extension of the MSSM is one of the simplest options to alleviate the little hierarchy problem [1, 2].
- (iii) Composite Higgs models (CHM). The scalar sector of most CHMs is non minimal. It includes a hyperchargeless triplet in one of the two simplest cosets admitting an UV completion *à la* QCD in four dimensions, viz. $SU(5)/SO(5)$ [3, 4]. Moreover, models based on $SO(7)/G_2$ [5] provide exactly one triplet in addition to the Higgs boson.

Therefore, the phenomenology of such triplet is not dictated by the renormalizable Lagrangian. The latter has to be instead supplemented with effective operators encoding the effects of the heavier resonances (SUSY partners, composite states, etc.), which can modify drastically the dynamics of Φ . To demonstrate this, we will work under the assumption that the triplet does not get a (custodial symmetry breaking) vacuum expectation value (VEV). This limit can be naturally enforced assuming the triplet is a CP-odd scalar and CP is conserved in the Higgs sector. At the renormalizable level, the Lagrangian becomes accidentally \mathbb{Z}_2 symmetric,

i.e. $\Phi \rightarrow -\Phi$, making the neutral component of the triplet a potential dark matter candidate. The charged components are in turn long-lived. The corresponding phenomenology has been studied in Refs. [6–8]. However, the effective operators make all components decay promptly even if the cutoff is $f \sim$ several TeV at which new resonances are out of the reach of current facilities. A much larger cutoff would introduce too large corrections also to the triplet mass, worsening the hierarchy problem.¹ In this article, we study probes of current and future colliders to this more natural version of the inert triplet model (ITM).

The extended Higgs sector modifies also the electroweak (EW) phase transition (EWPT). Thus, we extend previous studies in this respect [10, 11] computing the reach of future detectors for gravitational waves that originate in the production, evolution and eventual collisions of bubbles of vacuum in a first-order phase transition. The paper is organized as follows. We introduce the model in Sect. 2. We discuss the dynamics of the EWPT in Sect. 3. We explore collider signatures in Sect. 4. In Sect. 5 we propose an LHC analysis that has not been yet worked out experimentally for probing the key channel $pp \rightarrow t\bar{b}(\bar{t}b), b\bar{b}$. We study signal and background and provide prospects for the HL-LHC, namely the LHC running at a center of mass energy (c.m.e) $\sqrt{s} = 13$ TeV with integrated luminosity $\mathcal{L} = 3 \text{ ab}^{-1}$. We conclude in Sect. 6.

2 Model

The Lagrangian of the CP-odd scalar triplet when it is assumed embedded in an UV theory, takes the form:

$$L = \frac{1}{2} |D_\mu \Phi|^2 - \left\{ \frac{1}{2} \mu_\Phi^2 |\Phi|^2 + \frac{1}{2} \lambda_{H\Phi} |H|^2 |\Phi|^2 + \frac{1}{4} \lambda_\Phi |\Phi|^4 \right\} + \frac{1}{f} \left\{ i \bar{q}_L^i \left[c_{ij}^u (\tilde{H} \Phi) u_R^j + c_{ij}^d (H \Phi) d_R^j \right] + \text{h.c.} \right\}, \quad (1)$$

where $H = (h^+, h_0 = (h+v)/\sqrt{2})$ and $\Phi = (\phi^+, -\phi^0, \phi^-)$. We will assume flavour diagonal couplings: $c_{ij}^{u(d)} \sim c y_{u(d)} \delta_{ij}$ with c a constant and y Yukawa. We will comment on departures from this assumption in the conclusions. The relevant parameter is therefore the ratio c/f . The product $\tilde{H} \Phi$ ($H \Phi$) stands for the doublet in the $SU(2)_L \times U(1)_Y$ decomposition $2_{-(+)1/2} \times 3_0 = 2_{-(+)1/2} + 4_{-(+)1/2}$. Explicitly:

$$\tilde{H} \Phi = \begin{pmatrix} \phi_0 h_0^* - \sqrt{2} \phi^+ h^- \\ \phi_0 h^- - \sqrt{2} \phi^- h_0^* \end{pmatrix}, \quad (2)$$

¹ (The fine-tuning scales roughly as $\Delta \sim m_h^2/f^2$, with m_h the Higgs mass [9]. $f = 1 \text{ TeV}$ gives already $\Delta \sim 1\%$, and this falls below the permille level for $f > 4 \text{ TeV}$.)

and analogously for $H \Phi$ upon the replacement $h_0^* \rightarrow h^+$ and $h^- \rightarrow -h_0$. Therefore, in the unitary gauge after EWSB, we obtain:

$$L \supset \frac{v}{\sqrt{2}f} c \left\{ i y^t \phi_0 \bar{t} \gamma_5 t - i y^b \phi_0 \bar{b} \gamma_5 b \right. \quad (3)$$

$$\left. \times \left[-\sqrt{2} i \phi^- \bar{b} (y^t P_R + y^b P_L) t + \text{h.c.} \right] \right\}, \quad (4)$$

with $v \sim 246 \text{ GeV}$ and the sum extends to the first and second families of quarks, that we will denote collectively by q . Couplings to the leptons could be also present. We neglect them in this analysis.

$\phi^{0(\pm)}$ can decay into SM quarks. Likewise, for $m_t > m_\Phi$, the top quark can decay into the triplet and a bottom quark. (m_t stands for the top quark mass, whereas m_Φ is the physical mass of Φ ; at tree level $m_\Phi^2 = \mu_\Phi^2 + \lambda_{H\Phi} v^2/2$.) The following relations hold:

$$\Gamma(\phi_0 \rightarrow q\bar{q}) = \frac{3 y_q^2 v^2}{16\pi} \frac{c^2}{f^2} m_\Phi \sqrt{1 - \frac{4m_q^2}{m_\Phi^2}}, \quad (5)$$

$$\Gamma(\phi^+ \rightarrow q\bar{q}') = \frac{3(y_q^2 + y_{q'}^2) v^2}{16\pi} \frac{c^2}{f^2} m_\Phi \left[1 - \frac{m_q^2}{m_\Phi^2} \right]^2, \quad (6)$$

$$\Gamma(t \rightarrow \phi^+ b) = \frac{(y_b^2 + y_t^2) v^2}{32\pi} \frac{c^2}{f^2} m_t \left[1 - \frac{m_\Phi^2}{m_t^2} \right]^2. \quad (7)$$

In the second equation we are assuming $m_q \gg m_{q'}$, which is normally the case if the former is an up quark and the later a down quark. Note that decays into the light quarks are dominant if channels involving the top quark are kinematically closed. Partial widths as a function of m_Φ are depicted in Fig. 1.

Note also that, had we assumed a CP violating trilinear term in the potential, $\sim \kappa \Phi H^2$, this term would induce a VEV for the triplet, $v' \sim \kappa v^2/m_\Phi^2$. The triplet could also

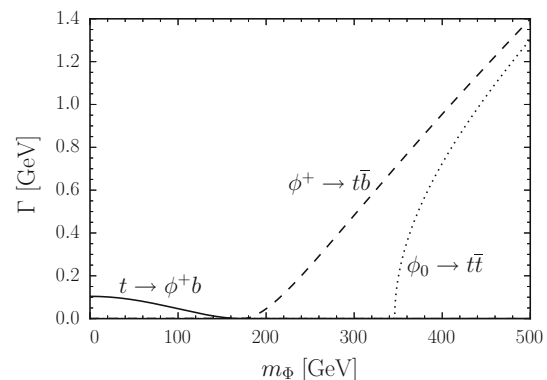


Fig. 1 Exotic decay widths of the different heavy particles in our model for $f = 1 \text{ TeV}$

decay into the Higgs degrees of freedom, the corresponding width scaling as $\Gamma \sim (v'/v^2)^2 m_\Phi^3$. Given that v' modifies the ρ parameter, it is bounded to be $v' \lesssim \text{GeV}$ [12]. Therefore, the corresponding decay would still be subdominant with respect to those suppressed by v/f even for $f \sim 10 \text{ TeV}$.

This setup can be easily accommodated in a SUSY framework. The minimal model consists of the MSSM extended with a supermultiplet Σ with quantum numbers $(1, \mathbf{3})_0$; see Ref. [13]. The most general and renormalizable superpotential is the MSSM superpotential extended by

$$\Delta W = \mu H_1 H_2 + \lambda H_1 \Sigma H_2 + \frac{1}{2} \mu_\Sigma \text{tr} \Sigma^2, \quad (8)$$

with H_1 and H_2 the two doublet superfields. Likewise, the extra soft-breaking Lagrangian reads

$$L_{\text{SB}} = m_4^2 \text{tr} \Sigma^\dagger \Sigma + \left[B_\Sigma \text{tr} \Sigma^2 + \lambda A_\lambda H_1 \Sigma H_2 + \text{h.c.} \right]. \quad (9)$$

In the limit $\lambda \rightarrow 0$, $\lambda \mu_\Sigma \rightarrow \text{finite}$, the fermionic partner in Σ decouples and the model is approximately inert with

$$\mu_\Phi^2 \sim m_4^2 + \mu_\Sigma^2 + B_\Sigma \mu_\Sigma, \quad (10)$$

$$\kappa_\Phi \sim -\sqrt{2} \lambda \mu_\Sigma. \quad (11)$$

In the previous expression, κ_Φ stands for the trilinear coupling in $\kappa_\Phi \Phi H H_2$. (With a slight abuse of notation, we are denoting here by H_2 the scalar component of this superfield.) After integrating H_2 out, we get

$$\lambda_{H\Phi} \sim \frac{(\lambda \mu_\Sigma)^2}{m_2^2}, \quad \frac{c^{u(d)}}{f} \sim y_2^{u(d)} \frac{\lambda \mu_\Sigma}{m_2^2}, \quad (12)$$

with m_2 the mass of H_2 and $y_2^{u(d)}$ its Yukawa couplings.

The Lagrangian above can also arise naturally in CHMs, in which both H and Φ are pNGBs originated in the (approximate) symmetry breaking pattern $\mathcal{G} \rightarrow \mathcal{H}$ at a scale f at which a new strong sector confines. The smallest realization of this setup relies on $SO(7) \rightarrow G_2$. The global symmetry is only approximate because it is explicitly broken by loops of SM gauge bosons, as well as by linear mixings between the left- and right-handed top quark fields and composite operators $\mathcal{O}_{L,R}$. The latter transform in representations of $SO(7)$. If $\mathcal{O}_L \sim \mathbf{35}$ and $\mathcal{O}_R \sim \mathbf{1}$, one obtains the Lagrangian [14]

$$L \sim y_u \bar{q}_L \tilde{H} \left[1 + \frac{\gamma}{f} \Phi + \mathcal{O}(1/f^2) \right] u_R, \quad (13)$$

and similarly for other quarks. γ parametrises the degree of mixing of q_L with the two doublets in the $\mathbf{35}$. (Under G_2 , $\mathbf{35} = \mathbf{1} + \mathbf{7} + \mathbf{27}$, whereas $\mathbf{7} = (\mathbf{2}, \mathbf{2}) + (\mathbf{3}, \mathbf{1})$ and $\mathbf{27} = (\mathbf{1}, \mathbf{1}) + (\mathbf{2}, \mathbf{2}) + (\mathbf{3}, \mathbf{3}) + (\mathbf{4}, \mathbf{2}) + (\mathbf{5}, \mathbf{1})$ under the custodial symmetry group $SU(2)_L \times SU(2)_R$.)

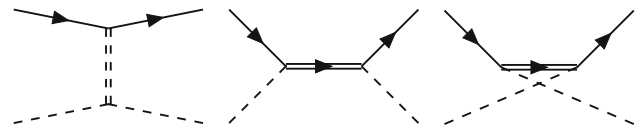


Fig. 2 Generation of the effective operator in Eq. 1 after integrating out a heavy scalar with with quantum numbers $(1, \mathbf{2})_{1/2}$ (left), a heavy vector-like quark $\sim (\mathbf{3}, \mathbf{3})_{-2/3 (1/3)}$ (center) or $\sim (\mathbf{3}, \mathbf{2})_{-1/6}$ (right) at a mass scale $M \sim f$. From left to right and top to bottom, the different fields are: q_L, t_R, H, Φ

The elementary ITM can also get $1/f$ corrections provided it is extended with new vector-like quarks with quantum numbers $(\mathbf{3}, \mathbf{3})_{-2/3 (1/3)}$, $(\mathbf{3}, \mathbf{2})_{-1/6}$; and/or with scalar doublets with quantum numbers $(1, \mathbf{2})_{1/2}$. The effective operator in Eq. 1 is then generated after integrating the heavy modes at the mass scale $M \sim f$; see Fig. 2. This list exhausts the possible tree-level weakly-coupled UV completions of the ITM that fit into our phenomenological framework.

LEP operated at $\sqrt{s} = 209 \text{ GeV}$, excluding Φ masses below $\sim 100 \text{ GeV}$. (This limit is however slightly model dependent; other sources of new physics could weaken it to even $\sim 75 \text{ GeV}$ [15].) We will therefore restrict our analysis to the mass range $100 < m_\Phi < 500 \text{ GeV}$.

3 The electroweak phase transition

The new scalar potential modifies the EWPT, which in the SM is a cross over. In the region of the parameter space where it is first order and strong, gravitational waves can be produced via nucleation and eventual collision of bubbles of symmetry-breaking vacuum. In order to explore this phenomenology, we study the evolution of the one-loop effective potential at finite temperature:

$$V = V_{\text{tree}} + \Delta V_{\text{CW}} + \Delta V_T + C. \quad (14)$$

C is a constant fixed so that V vanishes at the origin of the field space. V_{tree} stands for the tree-level potential. V_{CW} is the one-loop correction at zero temperature in $\overline{\text{MS}}$ and Landau gauge, namely

$$\Delta V_{\text{CW}} = \frac{1}{64\pi^2} \sum_i (\pm) n_i m_i^4 \left[\log \frac{m_i^2}{v^2} - c_i \right], \quad (15)$$

where i runs over all bosons (+) and fermions (−). The factor n_i denotes the number of degrees of freedom of the field i , while c_i is 5/6 for gauge bosons and 3/2 otherwise. The field-dependent masses squared of the spectator fields are

$$m_W^2 = \frac{1}{4} g^2 (h^2 + 4\phi_0^2), \quad (16)$$

$$m_Z^2 = \frac{1}{4} (g^2 + g'^2) h^2, \quad (17)$$

Table 1 Comparison of tree-level obtained parameters (0) versus the ones computed at one loop for different values of the three inputs

| m_Φ | $\lambda_{H\Phi}$ | λ_Φ | $(\mu_H^2)^0$ | $(\mu_\Phi^2)^0$ | λ_H^0 | μ_H^2 | μ_Φ^2 | λ_H |
|----------|-------------------|----------------|---------------|------------------|---------------|-----------|--------------|-------------|
| 120 | 1.1 | 1.1 | 7812.5 | -18883.8at | 0.13 | 9050.9 | -16600.6 | 0.127 |
| 200 | 2.0 | 1.0 | 7812.5 | -20516.0 | 0.13 | 8284.1 | -17069.8 | 0.125 |
| 320 | 3.5 | 1.5 | 7812.5 | -3503.0 | 0.13 | 5443.6 | 129.3 | 0.086 |
| 400 | 4.3 | 0.1 | 7812.5 | 29890.6 | 0.13 | 3583.3 | 29765.1 | 0.032 |
| 460 | 4.9 | 0.1 | 7812.5 | 63335.8 | 0.13 | 2693.4 | 61181.1 | -0.024 |

$$m_{G^{0,\pm}}^2 = -\mu_H^2 + \lambda_H h^2 + \frac{1}{2} \lambda_{H\Phi} \phi_0^2, \quad (18)$$

$$m_{\phi^\pm}^2 = \mu_\Phi^2 + \frac{1}{2} \lambda_{H\Phi} h^2 + \lambda_\Phi \phi_0^2, \quad (19)$$

$$m_t^2 = \frac{1}{2} y_t^2 h^2. \quad (20)$$

In addition, we have two more field dependent masses squared, m_1^2 and m_2^2 , given by the eigenvalues of the mixing matrix

$$\mathcal{M}^2 = \begin{bmatrix} -\mu_H^2 + 3\lambda_H h^2 + \frac{1}{2} \lambda_{H\Phi} \phi_0^2 & \lambda_{H\Phi} h \phi_0 \\ \lambda_{H\Phi} h \phi_0 & \mu_\Phi^2 + 3\lambda_\Phi \phi_0^2 + \frac{1}{2} \lambda_{H\Phi} h^2 \end{bmatrix} \quad (21)$$

Finally, the finite temperature corrections read

$$\Delta V_T = \frac{T^4}{2\pi^2} \sum_i (\pm) n_i \int_0^\infty y^2 \log \left[1 \mp e^{-\sqrt{\frac{m_i^2}{T^2} + y^2}} \right]. \quad (22)$$

As input parameters, we take m_Φ , $\lambda_{H\Phi}$ and λ_Φ . The remaining three parameters in the tree level potential are numerically obtained after requiring $V_{\text{tree}} + \Delta V_{\text{CW}}$ to have an extreme at $\langle h \rangle = v$, $\langle \phi_0 \rangle = 0$, at which the physical Higgs and Φ masses are $m_h \sim 125$ GeV and m_Φ , respectively. In other words:

$$\frac{\partial V}{\partial h} = 0, \quad \frac{\partial^2 V}{\partial h^2} = m_h^2, \quad \frac{\partial^2 V}{\partial \phi_0^2} = m_\Phi^2. \quad (23)$$

At tree level, $(v, 0)$ is guaranteed to be an extreme provided $\lambda_\Phi, \lambda_{H\Phi} > 0$ and $\mu_\Phi^2 > -1/2 v^2 \lambda_{H\Phi}$. A comparison between tree and loop level values of μ_H , μ_Φ and λ_H in a set of benchmark inputs can be seen in Table 1.

At high temperatures, the EW symmetry is restored. For certain values of the model parameters, the transition between $\langle h \rangle = 0 \rightarrow \langle h \rangle = v_n$ is not smooth as in the SM, but rather first order. One example is given in Fig. 3. In this case, the EWPT proceeds in two steps. An example of a first-order EWPT in one step is shown in Fig. 4. We will denote by T_n the nucleation temperature, namely the temperature at which the Higgs first order phase transition takes place. This is determined by the condition $S_3/T_n \sim 100$, where S_3 stands for the action of the thermal transition between vacua [16, 17].

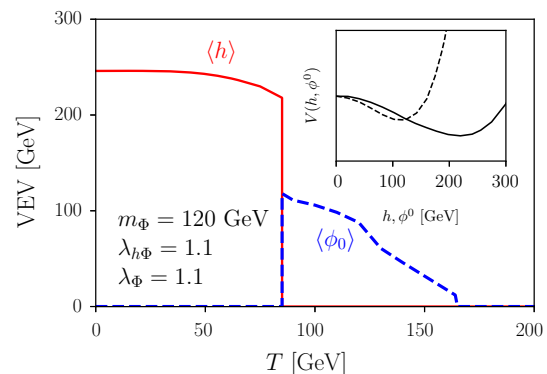


Fig. 3 Evolution of the VEV with the temperature for the parameter space point $m_\Phi = 120$ GeV, $\lambda_{H\Phi} = 1.1$, $\lambda_\Phi = 1.1$. At high temperatures, the EW symmetry is restored. It is spontaneously broken to $(\langle h \rangle, \langle \phi_0 \rangle) \sim (0, 10)$ GeV at $T \sim 160$ GeV, evolving until $T_n \sim 85$ GeV at which the step $(0, 120) \rightarrow (220, 0)$ GeV takes place. This latter transition is clearly strong; $\langle h \rangle/T_n > 1$. The shape of the potential T_n is also shown

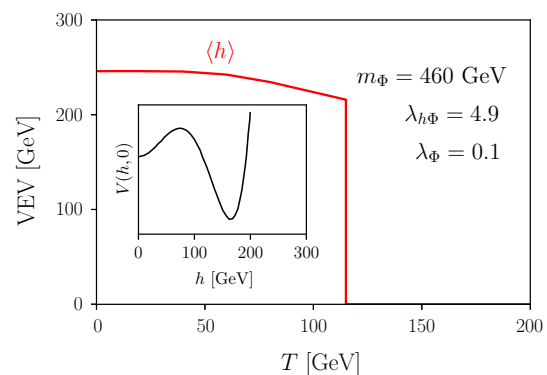


Fig. 4 Same as Fig. 3 but for the parameter space point $m_\Phi = 460$ GeV, $\lambda_{H\Phi} = 4.9$, $\lambda_\Phi = 0.1$. The EWPT proceeds in one step at $T_n = 115$ GeV in this case. $\langle \phi_0 \rangle$ vanishes for all values of T

In the region enclosed by the dashed green line in the plane $(\lambda_{H\Phi}, m_\Phi)$ of Fig. 5, $v_n/T_n > 1$; i.e. the phase transition is said to be *strong*. The nature of the strongest phase transition (one or two steps) is also labelled. The way we performed the scan is as follows: We varied m_Φ in the range [100, 500] GeV in steps of 20 GeV. We varied $\lambda_{H\Phi}$ in the range [0.1, 10] in steps of 0.1. For each pair $(m_\Phi, \lambda_{H\Phi})$, we found the value of λ_Φ in [0.1, 0.3, ..., 10] maximizing v_n/T_n . The points with

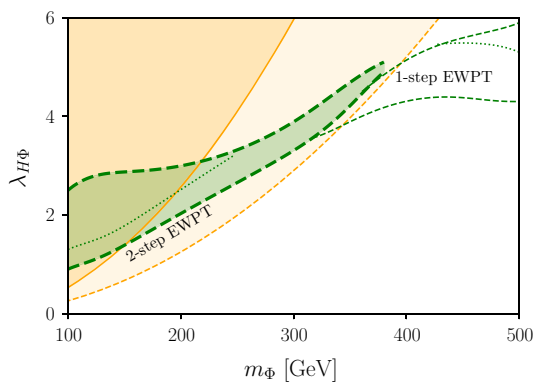


Fig. 5 The region in the plane $(m_\Phi, \lambda_{H\Phi})$ where the EWPT is strongly first order is enclosed by the two dashed green lines, each one labeling the structure of the phase transition (1- or 2-step). The sub-regions above the dotted lines can be tested at LISA. The area enclosed by the solid (dashed) orange line is (could be) excluded at the 95 % CL by current (future) measurements of the Higgs to photon width

smallest value of $\lambda_{H\Phi}$ are interpolated using straight lines. Likewise for those with largest value of this coupling. The resulting lines are further smoothed according to the *bezier* method using *Gnuplot*.

Note that at $T > 0$, the triplet squared term reads $\sim \mu_\Phi^2 + T^2$, which can not be negative for any value of $\mu_\Phi^2 > 0$. Therefore, the 2-step EWPT can only occur if the triplet minimum is present at $T = 0$. Moreover, for a fixed m_Φ , there is a minimum $\lambda_{H\Phi}$ below which μ_Φ^2 is not negative. Likewise, there is a maximum value of the coupling above which the potential at the triplet minimum, $V(0, \langle \phi_0 \rangle) \sim -|\mu_\Phi|^4/\lambda_\Phi$, is deeper than the Higgs one, the theory being therefore unstable. Altogether, they explain the bounded shape of the figure above.

It is also well known that strong first order phase transition, resulting from non-standard Higgs sectors, produce gravitational waves [18–47]. They are roughly characterized by the normalized latent heat of the phase transition

$$\alpha \sim \frac{\epsilon(T_n)}{35T_n^4}; \quad (24)$$

(with $\epsilon(T_n)$ the latent heat at T_n), and by the inverse duration time of the phase transition,

$$\frac{\beta}{H} \sim T_n \frac{d}{dT} \frac{S_3}{T} \sim T_n \frac{\Delta(S_3/T)}{\Delta T}. \quad (25)$$

We computed these quantities using *CosmoTransitions* [48]. $\Delta(S_3/T)$ is estimated finding the two values of T for which $S_3/T = 100, 200$ GeV, respectively. (Therefore, $\Delta(S/T) = 100$ GeV.) We warn that, due to the rapid growth of S_3/T with T , the linear estimation of the derivative can be sensibly overestimated. Given that small values of β/H give rise to stronger gravitational waves, our results are conservative. The region of the parameter space that we estimate it can be tested by the future gravitational wave observatory

LISA lies above the dotted green line in Fig. 5. The points in this are lead to α, β within the region “C1” of Ref. [21] for $T_n = 100$ GeV. (The bubble velocity is close to unity in good approximation. Also, we have neglected the effect that sounds waves might be not “long-lasting”, what could weaken the gravitational wave signal [49].)

Large values of $\lambda_{H\Phi}$ can be also probed in the $h \rightarrow \gamma\gamma$ channel. Indeed, the width of the later in this case reads

$$\Gamma(h \rightarrow \gamma\gamma) = \frac{\alpha^2 m_h^3}{1024\pi^3} \left\{ \frac{2}{v} \left[A_1(\tau_W) + \frac{4}{3} A_{1/2}(\tau_t) \right] + \lambda_{H\Phi} \frac{v}{m_\Phi^2} A_0(\tau_\Phi) \right\}^2, \quad (26)$$

with α the electromagnetic constant and $\tau_i = 4m_i^2/m_h^2$. The last ATLAS+CMS combined measurement of the Higgs decay into photons was provided in Ref. [50], $\Gamma(h \rightarrow \gamma\gamma)/\Gamma(h \rightarrow \gamma\gamma)_{\text{SM}} = 1.14_{-0.18}^{+0.19}$. The region in the plane $(m_\Phi, \lambda_{H\Phi})$ that is consequently excluded at the 95 % CL is enclosed by the solid orange line in Fig. 5. The expectation at the HL-LHC is that ratios outside the range 1.0 ± 0.1 will be excluded [51]. The corresponding region is enclosed by the dashed orange line. It is clear that, if departures from the SM prediction on the Higgs to diphoton rate are not observed, only one-step EWPT (*i.e.* single peak signatures) could be detected by LISA.

Finally, let us very briefly comment on the possibility of EW baryogenesis [52–55]. In our scenario, CP is violated spontaneously during the second transition in the two-step case, when both h and ϕ_0 change VEV and therefore the top mass acquires a CP violating phase. In related models [56] (see also Refs. [32, 57, 58]), EW baryogenesis has been shown successful provided $c\Delta v/f \gtrsim 0.1$, with Δv the change in VEV during the EWPT. In our case, Δv can be easily $\gtrsim 100$ GeV (see Fig. 3) and therefore $c\Delta v/f \gtrsim 0.1$ for $c/f \sim 1 \text{ TeV}^{-1}$.

A small explicit CP violating potential $\Delta V/T_n^4 \gg H/T_n \sim 10^{-16}$, with the Hubble scale H , is only needed to avoid domain wall problems [56]. In our setup, this can be triggered by a small CP-violating term in the potential, $\sim \kappa \Phi H^2$. At leading order in κ , it reflects in the (finite-temperature) potential as $V \sim \kappa T^3/(4\pi)^2$. Avoiding domain walls then implies $\kappa \gtrsim 10^{-12}$ GeV.

Let us show that this amount of CP violation evades easily neutron and electron dipole moment (EDM) constraints. Indeed, the neutron EDM arises mainly from the running of the diagram on the right panel of Fig. 6. It gives [59]

$$\left| \frac{d_n}{e} \right| \sim 20 \text{ MeV} \frac{g_3^3}{(4\pi)^4} \frac{y_t^2 v^2}{m_t^2 m_\Phi^2} \frac{c\kappa}{f} h(m_t^2/m_h^2), \quad (27)$$

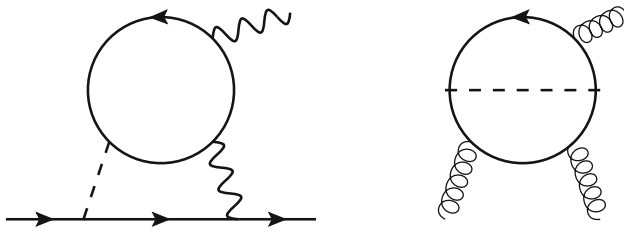


Fig. 6 Main contribution to the electron (left) and neutron (right) EDMs in the scalar triplet extension of the SM with a low cutoff

with g_3 the QCD coupling at the scale ~ 1 GeV, and

$$h(z) = z^2 \int_0^1 dx \int_0^1 dy \frac{x^3 y^3 (1-x)}{[zx(1-xy) + (1-x)(1-y)]^2}. \quad (28)$$

For the values of c/f and κ stated previously we obtain $|d_n| \sim 10^{-38}$ e cm, much smaller than the current 90% CL bound 2.9×10^{-26} e cm [60].

An electron EDM will be generated mainly via two-loop diagrams as that depicted in the left panel of Fig. 6. Using the expressions of Ref. [61], we find that the value of the electron EDM in our case reads

$$\frac{d}{e} \sim \frac{\alpha v^2 c}{6\pi^3 m_t f} y_t \frac{\kappa y_e}{m_\Phi^2} \left[f(m_t^2/m_h^2) + g(m_t^2/m_h^2) \right], \quad (29)$$

with

$$f(z) = \frac{1}{2} z \int_0^1 \frac{1-2x(1-x)}{x(1-x)-z} \log \frac{x(1-x)}{z} dx, \quad (30)$$

$$g(z) = \frac{1}{2} z \int_0^1 \frac{1}{x(1-x)-z} \log \frac{x(1-x)}{z} dx. \quad (31)$$

We obtain $|d_e| \sim 10^{-42}$ e cm, much smaller than the latest measurement by ACME [62], $d < 1.1 \times 10^{-29}$ e cm.

Regarding c/f , more stringent bounds could be set at colliders. We dedicate next section to this point.

4 Collider signatures

The scalar triplet can be produced at pp colliders in a variety of ways; see Fig. 7. The corresponding cross sections at $\sqrt{s} = 8, 13$ TeV are given in Fig. 8. For completeness, we also provide numbers for 27 and 100 TeV center-of-mass energy.

The triplet can be singly produced in $q\bar{q}$ initiated processes. The Yukawa suppression, together with the $1/f$ factor, makes the production cross section in this channel very small, though. Still, ϕ_0 can be singly produced in gluon fusion. In the regime $m_\Phi < 2m_t$, the most constraining searches are those looking for single production of $b\bar{b}$ resonances. The most up-to-date such analysis was recently

released by CMS; see Ref. [66]. It is based on 35.9 fb^{-1} of integrated luminosity collected at $\sqrt{s} = 13$ TeV. The region of the plane $(m_\Phi, c/f)$ that is excluded by this analysis is enclosed by the solid blue line in Fig. 9. It is expected that they become a factor of $\sqrt{3} \text{ fb}/35.9 \text{ ab} \sim 9$ stronger at the HL-LHC. The projected bound on the plane is enclosed by the dashed blue line in the same figure. For $m_\Phi > 2m_t$, ϕ_0 decays mostly into $t\bar{t}$. There are however no resonant searches for invariant masses below 500 GeV, neither at $\sqrt{s} = 8$ TeV nor $\sqrt{s} = 13$ TeV.

Moreover, the scalar triplet can be produced in association with top and bottom quarks, namely $pp \rightarrow \phi^+ t\bar{b}$. For $m_\Phi > m_t$, the most updated and constraining search is the ATLAS study of Ref. [67], which uses 36.1 fb^{-1} of LHC data collected at 13 TeV. It combines both the semi- and dileptonic channels. The limits on $\sigma(pp \rightarrow t\bar{b}\phi^\pm) \times \mathcal{B}(\phi^\pm \rightarrow t\bar{b})$ translate into the bounded region delimited by the green solid line in Fig. 9. A naive rescaling with the luminosity enhancement suggests that cross sections a factor of ~ 0.1 smaller can be tested at the HL-LHC. Translated to the plane $(m_\Phi, c/f)$, the corresponding bound is given by the region enclosed by the dashed line of the same colour.

In addition, for $m_t > m_\Phi$, the triplet can be also produced in the decay of the top quark. Current searches for $t\bar{t}$ production with $t \rightarrow \phi^\pm b$, $\phi^\pm \rightarrow jj$ have been carried out in CMS at $\sqrt{s} = 8$ TeV with an integrated luminosity of $\mathcal{L} = 19.7 \text{ fb}^{-1}$ [65]. This latter reference sets an upper bound on this rare top decay of $\mathcal{B}(t \rightarrow \phi^\pm b, \phi^\pm \rightarrow jj) < 1\text{--}2\%$ for $m_\Phi \sim 100\text{--}160$ GeV. Using Eq. 5, this constraint translates into the region enclosed by the solid red line in Fig. 9. The projected bound at the HL-LHC is depicted, too.

Finally, irrespectively of the value of c/f , the scalar triplets can be always pair-produced via EW charged currents (CC), $pp \rightarrow W^{\pm(*)} \rightarrow \phi^\pm \phi_0$, as well as via neutral currents (NC), $pp \rightarrow Z/\gamma \rightarrow \phi^+ \phi^-$. (Note that ϕ_0 does not interact with the Z boson and therefore it can not be pair-produced via NCs.) For $m_\Phi < m_t$, the new charged and neutral scalars decay mainly into $q'\bar{q}$ and $b\bar{b}$, respectively. Searches for pair-produced dijet resonances might therefore be sensitive to this regime. The most constraining such search is the CMS analysis presented in Ref. [68]. At this mass scale, each pair of quarks is very collimated and manifests as a single jet. The experimental analysis uses boosted techniques, including jet grooming to remove QCD radiation. The analysis considers $\mathcal{L} = 35.9 \text{ fb}^{-1}$ at 13 TeV of c.m.e. The current limits on the total cross section range from ~ 170 pb (100 GeV) to ~ 20 pb (170 GeV). Therefore, the parameter space of our model is not constrained. Furthermore, a naive rescaling with the larger luminosity shows that this analysis will not be even constraining at the HL-LHC.

For $m_t < m_\Phi < 2m_t$, the NC process gives rise to the final state $t\bar{b}, \bar{t}b$. The latest analysis exploring this channel for masses below 500 GeV was performed by CMS at $\sqrt{s} = 8$

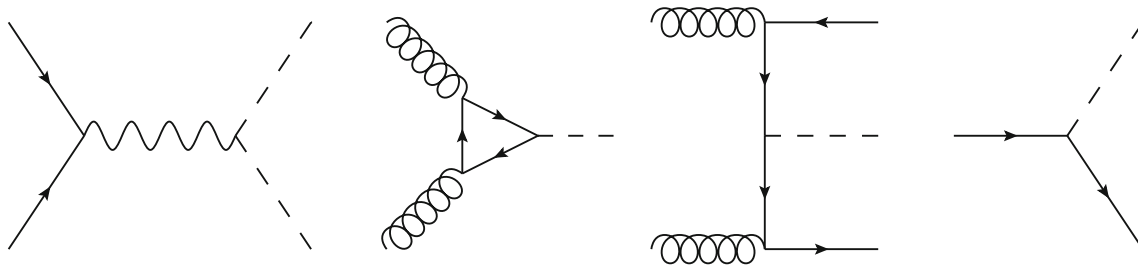


Fig. 7 Representative diagrams of the main Φ production mechanisms at pp colliders. Left) Pair production via EW currents. Middle-left) Single production via gluon fusion. Middle-right) Production in association with $t\bar{b}$ ($t\bar{b}$). Right) Production from the decay of a top quark

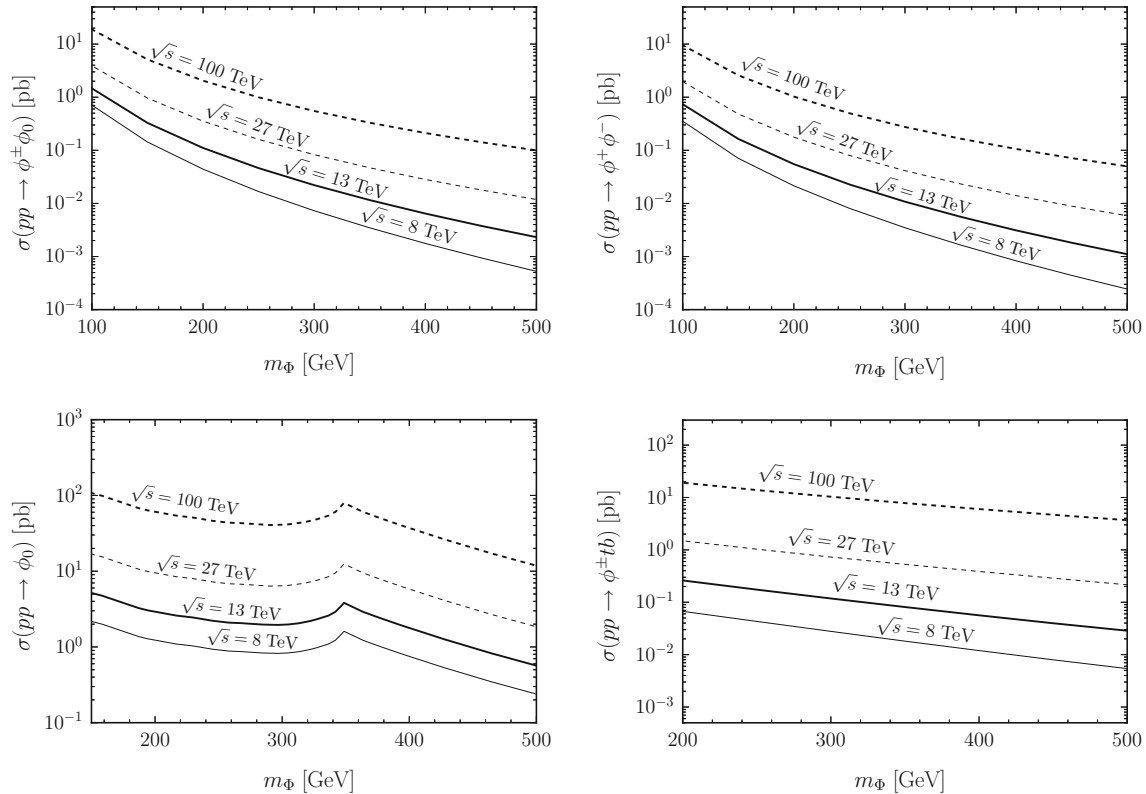


Fig. 8 Cross section of the different production modes for Φ at pp colliders of different c.m.e. The coupling c/f is set to 1TeV^{-1} . The production cross section of ϕ_0 via gluon fusion was rescaled from Ref. [63], at $\sqrt{s} = 13\text{ TeV}$. To obtain the cross sections for other c.m.e.,

we have computed the corresponding ratio in MadGraph, by using the Higgs EFT of the ggHFullLoop model. This ratio turns out to be a good approximation of the ratio in the full theory; see Ref. [64]

TeV; see Ref. [69]. Unfortunately, the corresponding limits range from $\sim 2.5\text{ pb}$ (250 GeV) to $\sim 0.5\text{ pb}$ (500 GeV). No region in our parameter space can be even constrained at the HL-LHC. Likewise, the CC gives $t\bar{b}(t\bar{b})$, $b\bar{b}$. To the best of our knowledge, there is however no dedicated search for pair produced resonances decaying to these final states. Being this channel c/f independent, we perform a signal and background simulation of this process in Sect. 5.

For $m_\Phi > 2m_t$, the NCs still give resonant $t\bar{b}$, $b\bar{t}$. The CC channel instead results in $t\bar{t}$, $t\bar{b}(b\bar{t})$. Once more, no dedicated analysis exists for this final state. (The lack of analyses sen-

sitivity to similar final states has been also recently pointed out in Ref. [70] in the context of composite dark sectors.) However, in comparison to this one, the $t\bar{b}(b\bar{t})$, $b\bar{b}$ analysis is much cleaner. Furthermore, it probes the mass range where the 2-step EWPT, and therefore EW baryogenesis, can occur.

5 LHC sensitivity

EW pair production of $t\bar{b}(t\bar{b})$, $b\bar{b}$ resonances occurs naturally in broadly-studied models, such as the 2HDM. Moreover, the

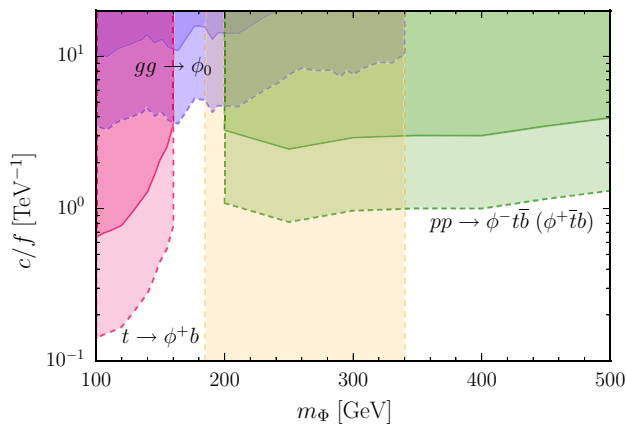


Fig. 9 Current (solid) and future (dashed) bounds on the parameter space (m_ϕ , c/f). The red region to the left comes from LHC searches for rare top decays, $t \rightarrow b\phi^\pm$, $\phi^\pm \rightarrow \text{jets}$; see Ref. [65]. The upper blue region comes from LHC searches for single production of $\phi^0 \rightarrow b\bar{b}$ via gluon fusion; see Ref. [66]. The green region to the right comes from LHC searches for single production of ϕ^\pm in association with a top and a bottom quark; see Ref. [67]. The middle vertical orange band is the region that could be tested using our dedicated analysis

cross section is independent of scalar to fermion couplings, provided the former decay promptly. It is therefore surprising that no experimental search has explored this channel at the LHC yet.

A plausible explanation is that the majority of these analyses are based on the 2HDM of the MSSM. In that case, one Higgs doublet gives mass to the up fermions, while the second gives mass to the down fermions. The physical charged components then couple to the top and bottom quarks with effective $c/f \sim (y_t \cot \beta + y_b \tan \beta)/v$, with $\tan \beta$ the ratio of the two doublet VEVs. Therefore, $c/f \geq 2\sqrt{y_b y_t}/v \sim 1 \text{ TeV}^{-1}$, the inequality being saturated at $\tan \beta = \sqrt{y_t/y_b} \sim 1.3$. As it can be seen in Fig. 9, this value is at the reach of $b\bar{b}$ resonant searches. Therefore, there is *a priori* no need for further analyses. The situation in our model and in other versions of the 2HDM is very different, though, because the coupling of the new scalars to the SM fermions can be (and typically is) very small. In the composite Higgs scenario, the effective scalar-fermion coupling can also be small, *i.e.* $c/f \lesssim 1 \text{ TeV}^{-1}$, according to Eq. 13 for natural values of $0 < \gamma \leq 1$.

With the aim of filling this gap, we perform a dedicated analysis for the process $pp \rightarrow \phi^\pm \phi_0 \rightarrow t\bar{b}(\bar{t}b), b\bar{b}$. We generate the hard processes for signal and background using MadGraph v5 [71] and shower them to a fully hadronised final state using Pythia v8 [72]. No parton-level cuts are applied. The main backgrounds are $t\bar{t} + \text{jets}$, $t\bar{t}b\bar{b}$, $t(\bar{t}) + 3b$ and $W + 4b$.

At the reconstruction level, a lepton is considered isolated if the hadronic energy deposit within a cone of size $R = 0.3$ is smaller than 10 % of the lepton candidate's p_T . Jets are

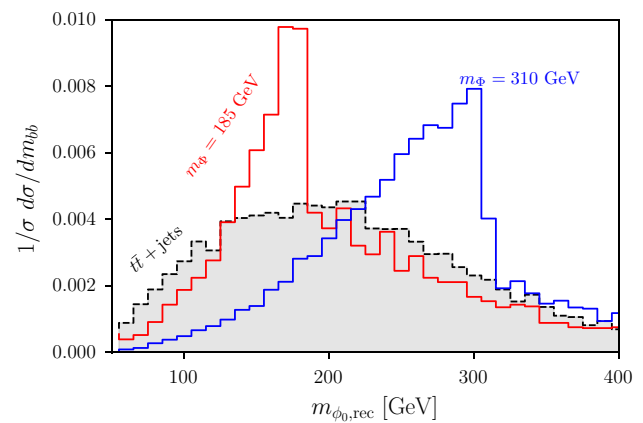


Fig. 10 Normalized distribution of $m_{\phi_0, \text{rec}}$ in the main background (dashed black) and in the signal for $m_\phi = 185 \text{ GeV}$ (solid red) and $m_\phi = 310 \text{ GeV}$ (solid blue)

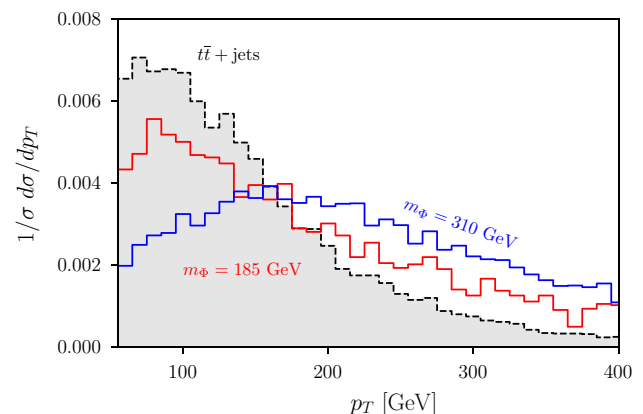


Fig. 11 Same as Fig. 10 but for p_T of the reconstructed ϕ^0

defined by the anti- k_T algorithm with $R = 0.4$. The following cuts are imposed:

1. Exactly one isolated lepton with $|y| < 2.5$ and $p_T > 15 \text{ GeV}$;
2. At least four jets, with $p_T > 30 \text{ GeV}$.

The longitudinal component of the missing neutrino is reconstructed using the requirement $m_W^2 = (p_l + p_\nu)^2$, with m_W the mass of the W boson. The neutrino and lepton four-momenta, p_ν and p_l , are then added to the jet which gives a total invariant mass closest to the top quark mass. After this,

3. The invariant mass of this top is required to be within 50 GeV of the top mass;
4. Three b -tagged jets are to be found among the jets not coming from the leptonic top.
5. We require the reconstructed masses of ϕ_0 and ϕ^\pm to be similar, *i.e.* $|m_{\phi_0, \text{rec}} - m_{\phi^\pm, \text{rec}}| \leq 50 \text{ GeV}$.

Table 2 Top) Effective cross section in fb for the signal (for $m_\phi = 185$ GeV) and the backgrounds after each cut (1 – 5), as described in the text. Bottom) Effective cross section in fb after all cuts, including cut

6, for different signals and for the total background. The sensitivity at the HL-LHC is also shown

| Cuts | $m_\phi = 185$ | $t\bar{t} + \text{jets}$ | $t + 3b$ | $t\bar{t}b\bar{b}$ | $W + 4b$ |
|--------------|----------------|--------------------------|----------|--------------------|----------|
| iso. lepton | 72.94 | 96693.1 | 0.65632 | 326.72 | 1.327 |
| nr. jets | 29.71 | 55288.5 | 0.6834 | 305.10 | 0.6147 |
| lep. top | 17.69 | 32626.6 | 0.393 | 198.10 | 0.3647 |
| 3 b -tags | 2.3 | 267.4 | 0.07531 | 45.45 | 0.0835 |
| similar mass | 0.93 | 81.1 | 0.0235 | 12.35 | 0.0220 |
| Final rec | Signal | Background | | $s/\sqrt{s+b}$ | |
| $\Phi(185)$ | 0.39 | 25.6 | | 4.2 | |
| $\Phi(235)$ | 0.78 | 33.5 | | 7.3 | |
| $\Phi(285)$ | 0.41 | 26.5 | | 4.3 | |
| $\Phi(335)$ | 0.22 | 19.0 | | 2.7 | |

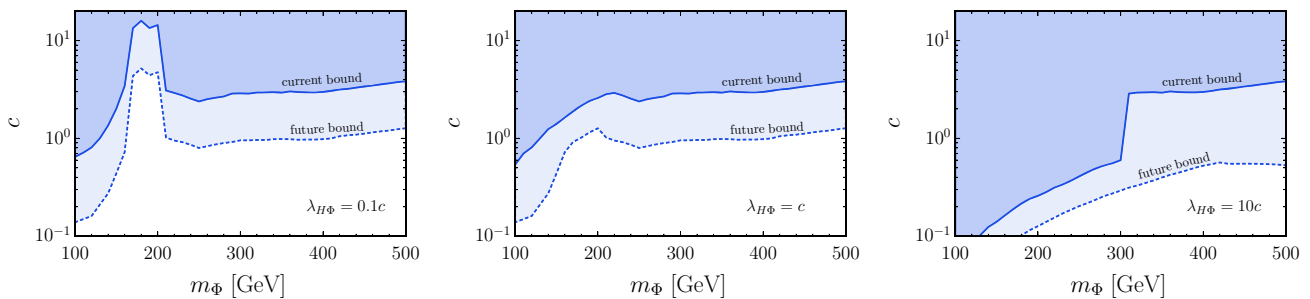


Fig. 12 Current (solid) and future (dashed) bounds on the plane (m_ϕ, c) for $\lambda_{H\phi} = 0.1c$ (left), $\lambda_{H\phi} = c$ (center) and $\lambda_{H\phi} = 10c$ (right) and $f = 1$ TeV

To decide which b -tagged jet is assigned to ϕ^\pm and which two are assigned to ϕ_0 , we compute all possible combinations and choose the one resulting in the minimum difference between $m_{\phi_0, \text{rec}}$ and $m_{\phi^\pm, \text{rec}}$. The normalized distribution of this former variable in the main background ($t\bar{t} + \text{jets}$) and in the signal for $m_\phi = 185$ GeV and $m_\phi = 310$ GeV is depicted in Fig. 10. In Fig. 11, we also show the normalized distribution of the p_T of the reconstructed ϕ^0 . However, cutting on this variable is costly in cross section, but would allow to improve the ratio of signal over background further.

Finally,

6. We reconstruct the resonances ϕ_0 and ϕ^\pm in the mass window of ± 30 and ± 40 GeV, respectively. As shown in Fig. 10 the experimental width of the resonances depends on their masses, thus, the central value of the mass window in the $(m_{\phi_0, \text{rec}}, m_{\phi^\pm, \text{rec}})$ plane has to be optimised for each m_ϕ separately.

The cut-flow for the signal and the relevant backgrounds is given in Table 2. The sensitivity estimates are conservative, as the reconstruction relies on fairly inclusive cuts using large mass windows. Further, it is likely that some of the background was counted twice, as b -quarks from the parton

shower in $t\bar{t}$ and from the matrix element in $t\bar{t}b\bar{b}$ are both contributing to the total background. Thus, we expect that the sensitivity can be improved further using a combination of multi-variate techniques [73–75] and high- p_T final states [76].

We estimate the sensitivity at the HL-LHC as $\mathcal{S} = s/\sqrt{s+b}$, with s and b the number of signal and background events after all cuts, respectively. It ranges from 2.7 to 7.3 for m_ϕ between 185 and 340 GeV. Thus, at the LHC ($\sqrt{s} = 13$ TeV) we can probe the entire mass interval with 3000 fb^{-1} . The corresponding region in the plane $(m_\phi, c/f)$ is therefore a vertical band, the one enclosed by the dashed orange line in Fig. 9.

6 Conclusions

Natural scalar extensions of the SM must have a low cutoff f preventing large corrections to the scalar masses. However, such models are usually studied neglecting $1/f$ terms. Basing on the real triplet extension of the SM, we have highlighted that, if these terms are taken into account, the phenomenology can be drastically different. In particular, the only renor-

malizable interaction allowing the new scalars to decay is so suppressed by the measurement of the ρ parameter, that decays mediated by effective operators dominate.

We have studied the reach of current LHC analyses. We have found that, despite being f independent, searches for EW pair-produced charged scalars decaying to third generation quarks are absent. This is particularly surprising given that such signals appear in a plethora of new physics models, including the 2HDM/MSSM. Therefore, we have developed a dedicated analysis to probe the cleanest of these channels: $pp \rightarrow \phi^\pm \phi_0 \rightarrow t\bar{b}(\bar{t}b), b\bar{b}$. We have shown that the whole range of masses $\sim 185\text{--}340$ GeV can be tested at the HL-LHC.

For this analysis, we have neglected new scalar couplings to the leptons. Under the sort of Minimal Flavour Violation [77] assumed after Eq. 1, explicitly reproduced in concrete models as shown in Eq. 13, the only relevant lepton would be the tau. Still, the decay of ϕ^0 into $\tau^+\tau^-$ would involve only a $\sim m_\tau^2/(m_b^2 N_c) \sim 5\%$ of its width; our results being effectively unaffected. If couplings to the leptons are accidentally larger, the scalar could be better seen elsewhere; see Ref. [78].

We also stress that, had he assume flavour-violating couplings $c_{ij}^{u(d)}$, they would give rise to a plethora of signals in meson decays [79]. They could be also seen in top decays as in the singlet extension of the Higgs sector [80].

On another front, we have studied the reach of the future gravitational wave observatory LISA to the gravitational waves produced in the EWPT for certain region of the parameter space of the model. In particular, we have demonstrated that regions not yet excluded by Higgs to diphoton measurements will be testable. In this region, the EWPT proceeds mainly in one step, and therefore only one signal peak might be expected.

Finally, it is worth mentioning that in concrete models c and $\lambda_{H\Phi}$ related; normally $\lambda_{H\Phi} \propto c$. This is evident for example in CHMs, in which the former (latter) is induced by integrating out heavier resonances at tree level (one loop). To exhaust this point, we plot in Fig. 12 the current and future bounds on the plane (m_ϕ, c) considering all collider searches and gravitational wave signatures for different simple assumptions on the relation $\lambda_{H\Phi} = \lambda_{H\Phi}(c)$.

Acknowledgements We would like to thank Nuno Castro, Marek Lewicki, Mariano Quirós and Carlos Tamarit for helpful discussions. MC is supported by the Royal Society under the Newton International Fellowship programme. MR is supported by Fundação para a Ciência e Tecnologia (FCT) under the Grant PD/BD/142773/2018 and also acknowledges financing from LIP (FCT, COMPETE2020-Portugal2020, FEDER, POCI-01-0145-FEDER-007334).

Data Availability Statement This manuscript has no associated data or the data will not be deposited. [Authors' comment: This paper is based on research in theoretical physics. Hence, there are no associated data to be deposited.]

Open Access This article is distributed under the terms of the Creative Commons Attribution 4.0 International License (<http://creativecommons.org/licenses/by/4.0/>), which permits unrestricted use, distribution, and reproduction in any medium, provided you give appropriate credit to the original author(s) and the source, provide a link to the Creative Commons license, and indicate if changes were made. Funded by SCOAP³.

Appendix A: Loop functions

In our case, $2m_\phi > m_h$, and therefore

$$\begin{aligned} A_0(x) &= -x^2 \left[x^{-1} - f(x^{-1}) \right], \\ A_{1/2}(x) &= 2x^2 \left[x^{-1} + (x^{-1} - 1)f(x^{-1}) \right], \\ A_1(x) &= -x^2 \left[2x^{-2} + 3x^{-1} + 3(2x^{-1} - 1)f(x^{-1}) \right] \end{aligned} \quad (\text{A1})$$

with

$$f(x) = \arcsin^2 \sqrt{x}. \quad (\text{A2})$$

References

1. J.R. Espinosa, M. Quiros, Higgs triplets in the supersymmetric standard model. Nucl. Phys. B **384**, 113–146 (1992)
2. S. Di Chiara, K. Hsieh, Triplet extended supersymmetric standard model. Phys. Rev. D **78**, 055016 (2008). [arXiv:0805.2623](#)
3. L. Vecchi, *The Natural Composite Higgs*. [arXiv:1304.4579](#)
4. G. Ferretti, Gauge theories of partial compositeness: scenarios for Run-II of the LHC. JHEP **06**, 107 (2016). [arXiv:1604.06467](#)
5. M. Chala, $h \rightarrow \gamma\gamma$ excess and dark matter from composite Higgs models. JHEP **01**, 122 (2013). [arXiv:1210.6208](#)
6. M. Cirelli, N. Fornengo, A. Strumia, Minimal dark matter. Nucl. Phys. B **753**, 178–194 (2006). [arXiv:hep-ph/0512090](#)
7. P. Fileviez Perez, H.H. Patel, M. Ramsey-Musolf, K. Wang, Triplet scalars and dark matter at the LHC. Phys. Rev. D **79**, 055024 (2009). [arXiv:0811.3957](#)
8. A. Carmona, M. Chala, Composite dark sectors. JHEP **06**, 105 (2015). [arXiv:1504.00332](#)
9. G. Panico, A. Wulzer, The composite Nambu-goldstone Higgs. Lect. Notes Phys. **913**, 1–316 (2016). [arXiv:1506.01961](#)
10. N. Blinov, J. Kozaczuk, D.E. Morrissey, C. Tamarit, Electroweak baryogenesis from exotic electroweak symmetry breaking. Phys. Rev. D **92**, 035012 (2015). [arXiv:1504.05195](#)
11. S. Inoue, G. Ovanessian, M.J. Ramsey-Musolf, Two-step electroweak baryogenesis. Phys. Rev. D **93**, 015013 (2016). [arXiv:1508.05404](#)
12. PARTICLE DATA GROUP collaboration, M. Tanabashi et al., Review of particle physics. Phys. Rev. D **98**, 030001 (2018)
13. A. Delgado, G. Nardini, M. Quiros, A light supersymmetric Higgs sector hidden by a standard model-like Higgs. JHEP **07**, 054 (2013). [arXiv:1303.0800](#)
14. G. Ballesteros, A. Carmona, M. Chala, Exceptional composite dark matter. Eur. Phys. J. C **77**, 468 (2017). [arXiv:1704.07388](#)
15. D. Egana-Ugrinovic, M. Low, J.T. Ruderman, Charged Fermions below 100 GeV. JHEP **05**, 012 (2018). [arXiv:1801.05432](#)

16. M. Quiros, *Finite temperature field theory and phase transitions*, in *Proceedings, Summer school in high-energy physics and cosmology: Trieste, Italy, June 29–July 17, 1998*, pp. 187–259, (1999). [arXiv:hep-ph/9901312](#)
17. M. Laine, A. Vuorinen, Basics of thermal field theory. *Lect. Notes Phys.* **925**, 1–281 (2016). [arXiv:1701.01554](#)
18. J. Choi, R.R. Volkas, Real Higgs singlet and the electroweak phase transition in the standard model. *Phys. Lett. B* **317**, 385–391 (1993). [arXiv:hep-ph/9308234](#)
19. A. Ashoorioon, T. Konstandin, Strong electroweak phase transitions without collider traces. *JHEP* **07**, 086 (2009). [arXiv:0904.0353](#)
20. K. Enqvist, S. Nurmi, T. Tenkanen, K. Tuominen, Standard model with a real singlet scalar and inflation. *JCAP* **1408**, 035 (2014). [arXiv:1407.0659](#)
21. C. Caprini, Science with the space-based interferometer eLISA. II: gravitational waves from cosmological phase transitions. *JCAP* **1604**, 001 (2016). [arXiv:1512.06239](#)
22. M. Kakizaki, S. Kanemura, T. Matsui, Gravitational waves as a probe of extended scalar sectors with the first order electroweak phase transition. *Phys. Rev. D* **92**, 115007 (2015). [arXiv:1509.08394](#)
23. P. Schwaller, Gravitational waves from a dark phase transition. *Phys. Rev. Lett.* **115**, 181101 (2015). [arXiv:1504.07263](#)
24. J. Jaeckel, V.V. Khoze, M. Spannowsky, Hearing the signal of dark sectors with gravitational wave detectors. *Phys. Rev. D* **94**, 103519 (2016). [arXiv:1602.03901](#)
25. F.P. Huang, Y. Wan, D.-G. Wang, Y.-F. Cai, X. Zhang, Hearing the echoes of electroweak baryogenesis with gravitational wave detectors. *Phys. Rev. D* **94**, 041702 (2016). [arXiv:1601.01640](#)
26. K. Hashino, M. Kakizaki, S. Kanemura, T. Matsui, Synergy between measurements of gravitational waves and the triple-Higgs coupling in probing the first-order electroweak phase transition. *Phys. Rev. D* **94**, 015005 (2016). [arXiv:1604.02069](#)
27. T. Tenkanen, K. Tuominen, V. Vaskonen, A strong electroweak phase transition from the inflaton field. *JCAP* **1609**, 037 (2016). [arXiv:1606.06063](#)
28. P. Huang, A.J. Long, L.-T. Wang, Probing the electroweak phase transition with Higgs factories and gravitational waves. *Phys. Rev. D* **94**, 075008 (2016). [arXiv:1608.06619](#)
29. M. Artymowski, M. Lewicki, J.D. Wells, Gravitational wave and collider implications of electroweak baryogenesis aided by non-standard cosmology. *JHEP* **03**, 066 (2017). [arXiv:1609.07143](#)
30. F.P. Huang, X. Zhang, Probing the gauge symmetry breaking of the early universe in 3-3-1 models and beyond by gravitational waves. *Phys. Lett. B* **788**, 288–294 (2019). [arXiv:1701.04338](#)
31. K. Hashino, M. Kakizaki, S. Kanemura, P. Ko, T. Matsui, Gravitational waves and Higgs boson couplings for exploring first order phase transition in the model with a singlet scalar field. *Phys. Lett. B* **766**, 49–54 (2017). [arXiv:1609.00297](#)
32. V. Vaskonen, Electroweak baryogenesis and gravitational waves from a real scalar singlet. *Phys. Rev. D* **95**, 123515 (2017). [arXiv:1611.02073](#)
33. W. Chao, H.-K. Guo, J. Shu, Gravitational wave signals of electroweak phase transition triggered by dark matter. *JCAP* **1709**, 009 (2017). [arXiv:1702.02698](#)
34. M. Hindmarsh, S.J. Huber, K. Rummukainen, D.J. Weir, Shape of the acoustic gravitational wave power spectrum from a first order phase transition. *Phys. Rev. D* **96**, 103520 (2017). [arXiv:1704.05871](#)
35. A. Kobakhidze, A. Manning, J. Yue, Gravitational waves from the phase transition of a nonlinearly realized electroweak gauge symmetry. *Int. J. Mod. Phys. D* **26**, 1750114 (2017). [arXiv:1607.00883](#)
36. A. Beniwal, M. Lewicki, J.D. Wells, M. White, A.G. Williams, Gravitational wave, collider and dark matter signals from a scalar singlet electroweak baryogenesis. *JHEP* **08**, 108 (2017). [arXiv:1702.06124](#)
37. A. Kobakhidze, C. Lagger, A. Manning, J. Yue, Gravitational waves from a supercooled electroweak phase transition and their detection with pulsar timing arrays. *Eur. Phys. J. C* **77**, 570 (2017). [arXiv:1703.06552](#)
38. R.-G. Cai, M. Sasaki, S.-J. Wang, The gravitational waves from the first-order phase transition with a dimension-six operator. *JCAP* **1708**, 004 (2017). [arXiv:1707.03001](#)
39. L. Bian, H.-K. Guo, J. Shu, Gravitational waves, baryon asymmetry of the universe and electric dipole moment in the CP-violating NMSSM. *Chin. Phys. C* **42**, 093106 (2018). [arXiv:1704.02488](#)
40. F.P. Huang, C.S. Li, Probing the baryogenesis and dark matter relaxed in phase transition by gravitational waves and colliders. *Phys. Rev. D* **96**, 095028 (2017). [arXiv:1709.09691](#)
41. D. Croon, V. Sanz, G. White, Model discrimination in gravitational wave spectra from dark phase transitions. *JHEP* **08**, 203 (2018). [arXiv:1806.02332](#)
42. A. Mazumdar, G. White, Cosmic phase transitions: their applications and experimental signatures. [arXiv:1811.01948](#)
43. K. Hashino, R. Jinno, M. Kakizaki, S. Kanemura, T. Takahashi, M. Takimoto, Fingerprinting models of first-order phase transitions by the synergy between collider and gravitational-wave experiments. [arXiv:1809.04994](#)
44. A. Ahriche, K. Hashino, S. Kanemura, S. Nasri, Gravitational waves from phase transitions in models with charged singlets. [arXiv:1809.09883](#)
45. A. Beniwal, M. Lewicki, M. White, A. G. Williams, Gravitational waves and electroweak baryogenesis in a global study of the extended scalar singlet model. [arXiv:1810.02380](#)
46. F.P. Huang, J.-H. Yu, Exploring inert dark matter blind spots with gravitational wave signatures. *Phys. Rev. D* **98**, 095022 (2018). [arXiv:1704.04201](#)
47. M. Breitbach, J. Kopp, E. Madge, T. Opferkuch, P. Schwaller, Dark, cold, and noisy: constraining secluded hidden sectors with gravitational waves. [arXiv:1811.11175](#)
48. C.L. Wainwright, CosmoTransitions: computing cosmological phase transition temperatures and bubble profiles with multiple fields. *Comput. Phys. Commun.* **183**, 2006–2013 (2012). [arXiv:1109.4189](#)
49. J. Ellis, M. Lewicki, J. M. No, On the maximal strength of a first-order electroweak phase transition and its gravitational wave signal. Submitted to: *JCAP*. (2018). [arXiv:1809.08242](#)
50. CMS collaboration, A. M. Sirunyan et al., *Combined measurements of Higgs boson couplings in proton–proton collisions at $\sqrt{s} = 13\text{ TeV}$* . Submitted to: *Eur. Phys. J.* (2018). [arXiv:1809.10733](#)
51. Projections for measurements of Higgs boson cross sections, branching ratios and coupling parameters with the ATLAS detector at a HL-LHC. Tech. Rep. ATL-PHYS-PUB-2013-014, CERN, Geneva, Oct (2013)
52. V.A. Kuzmin, V.A. Rubakov, M.E. Shaposhnikov, On the anomalous electroweak baryon number nonconservation in the early universe. *Phys. Lett. B* **155**, 36 (1985)
53. A.G. Cohen, D.B. Kaplan, A.E. Nelson, Progress in electroweak baryogenesis. *Ann. Rev. Nucl. Part. Sci.* **43**, 27–70 (1993). [arXiv:hep-ph/9302210](#)
54. A. Riotto, M. Trodden, Recent progress in baryogenesis. *Ann. Rev. Nucl. Part. Sci.* **49**, 35–75 (1999). [arXiv:hep-ph/9901362](#)
55. D.E. Morrissey, M.J. Ramsey-Musolf, Electroweak baryogenesis. *New J. Phys.* **14**, 125003 (2012). [arXiv:1206.2942](#)
56. J.R. Espinosa, B. Gripaios, T. Konstandin, F. Riva, Electroweak baryogenesis in non-minimal composite Higgs models. *JCAP* **1201**, 012 (2012). [arXiv:1110.2876](#)
57. F.P. Huang, Z. Qian, M. Zhang, Exploring dynamical CP violation induced baryogenesis by gravitational waves and colliders. *Phys. Rev. D* **98**, 015014 (2018). [arXiv:1804.06813](#)

58. B. Grzadkowski, D. Huang, Spontaneous CP -violating electroweak baryogenesis and dark matter from a complex singlet scalar. *JHEP* **08**, 135 (2018). [arXiv:1807.06987](#)
59. K. Choi, S.H. Im, H. Kim, D.Y. Mo, 750 GeV diphoton resonance and electric dipole moments. *Phys. Lett. B* **760**, 666–673 (2016). [arXiv:1605.00206](#)
60. C.A. Baker, An improved experimental limit on the electric dipole moment of the neutron. *Phys. Rev. Lett.* **97**, 131801 (2006). [arXiv:hep-ex/0602020](#)
61. V. Keus, N. Koivunen, K. Tuominen, Singlet scalar and 2HDM extensions of the standard model: CP-violation and constraints from $(g-2)_\mu$ and e EDM. *JHEP* **09**, 059 (2018). [arXiv:1712.09613](#)
62. ACME collaboration, V. Andreev et al., Improved limit on the electric dipole moment of the electron. *Nature* **562**, 355–360 (2018)
63. R. Primulando, P. Uttayarat, Probing lepton flavor violation at the 13 TeV LHC. *JHEP* **05**, 055 (2017). [arXiv:1612.01644](#)
64. Q. Li, M. Spira, J. Gao, C.S. Li, Higgs boson production via gluon fusion in the standard model with four generations. *Phys. Rev. D* **83**, 094018 (2011). [arXiv:1011.4484](#)
65. CMS collaboration, V. Khachatryan et al., Search for a light charged Higgs boson decaying to $c\bar{s}$ in pp collisions at $\sqrt{s} = 8\text{TeV}$, *JHEP* **12**, 178 (2015). [arXiv:1510.04252](#)
66. CMS collaboration, A. M. Sirunyan et al., Search for low-mass resonances decaying into bottom quark-antiquark pairs in proton–proton collisions at $\sqrt{s} = 13\text{TeV}$. [arXiv:1810.11822](#)
67. ATLAS collaboration, M. Aaboud et al., Search for charged Higgs bosons decaying into top and bottom quarks at $\sqrt{s} = 13\text{TeV}$ with the ATLAS detector. Submitted to: *JHEP*. (2018). [arXiv:1808.03599](#)
68. CMS collaboration, A. M. Sirunyan et al., Search for pair-produced resonances decaying to quark pairs in proton–proton collisions at $\sqrt{s} = 13\text{TeV}$. [arXiv:1808.03124](#)
69. CMS collaboration, C. Collaboration, Search for pair production of resonances decaying to a top quark plus a jet in final states with two leptons. CMS-PAS-B2G-12-008
70. G. D. Kribs, A. Martin, B. Ostidek, T. Tong, Dark Mesons at the LHC. [arXiv:1809.10184](#)
71. J. Alwall, R. Frederix, S. Frixione, V. Hirschi, F. Maltoni, O. Mattelaer, The automated computation of tree-level and next-to-leading order differential cross sections, and their matching to parton shower simulations. *JHEP* **07**, 079 (2014). [arXiv:1405.0301](#)
72. T. Sjstrand, S. Ask, J.R. Christiansen, R. Corke, N. Desai, P. Ilten et al., An introduction to PYTHIA 8.2. *Comput. Phys. Commun.* **191**, 159–177 (2015). [arXiv:1410.3012](#)
73. D.E. Soper, M. Spannowsky, Finding physics signals with shower deconstruction. *Phys. Rev. D* **84**, 074002 (2011). [arXiv:1102.3480](#)
74. D.E. Soper, M. Spannowsky, Finding top quarks with shower deconstruction. *Phys. Rev. D* **87**, 054012 (2013). [arXiv:1211.3140](#)
75. D.E. Soper, M. Spannowsky, Finding physics signals with event deconstruction. *Phys. Rev. D* **89**, 094005 (2014). [arXiv:1402.1189](#)
76. A. Abdesselam, Boosted objects: a probe of beyond the standard model physics. *Eur. Phys. J. C* **71**, 1661 (2011). [arXiv:1012.5412](#)
77. G. D'Ambrosio, G.F. Giudice, G. Isidori, A. Strumia, Minimal flavor violation: an effective field theory approach. *Nucl. Phys. B* **645**, 155–187 (2002). [arXiv:hep-ph/0207036](#)
78. A.G. Akeroyd, S. Moretti, M. Song, Light charged Higgs boson with dominant decay to quarks and its search at the LHC and future colliders. *Phys. Rev. D* **98**, 115024 (2018). [arXiv:1810.05403](#)
79. R. Harnik, J. Kopp, J. Zupan, Flavor violating higgs decays. *JHEP* **03**, 026 (2013). [arXiv:1209.1397](#)
80. S. Banerjee, M. Chala, M. Spannowsky, Top quark FCNCs in extended Higgs sectors. *Eur. Phys. J. C* **78**, 683 (2018). [arXiv:1806.02836](#)